Powder Technology 407 (2022) 117671

Contents lists available at ScienceDirect

Powder Technology

journal homepage: www.journals.elsevier.com/powder-technology

Chiral separation of rotating robots through obstacle arrays

Wenjian Li [a], Longfei Li [a,b], Qingfan Shi [a], Mingcheng Yang [b,c,d,*], Ning Zheng [a,**]

[a] School of Physics, Beijing Institute of Technology, Beijing 100081, China
[b] Beijing National Laboratory for Condensed Matter Physics and Laboratory of Soft Matter Physics, Institute of Physics, Chinese Academy of Sciences, Beijing 100190, China
[c] School of Physical Sciences, University of Chinese Academy of Sciences, Beijing 100049, China
[d] Songshan Lake Materials Laboratory, Dongguan, Guangdong 523808, China

HIGHLIGHTS

- We experimentally realize chiral sorting of active rotors by using obstacle array.
- A theoretical model is proposed to capture the essential mechanism of chiral sorting.
- The system has the potential to separate objects with static chiral structures.

GRAPHICAL ABSTRACT

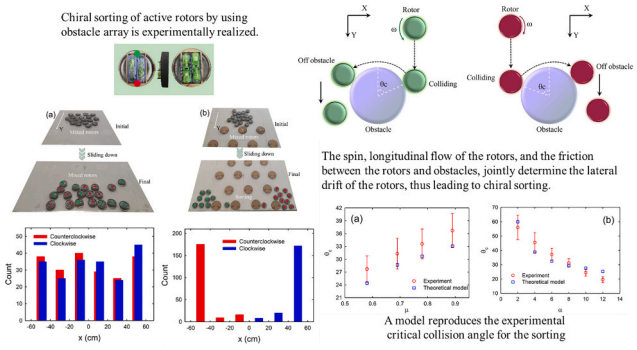

ARTICLE INFO

Keywords:
Active matter
Separation
Chirality
Artificial particles
Obstacle

ABSTRACT

The interplay between active matter and environmental complexity can be applied to achieve complex functions ranging from rectification, separation, and capture to sorting of active particles. Here, we experimentally realize chiral separation of disk-shaped active rotors by using the interactions between the rotors and the obstacle array. Differently chiral active particles passing through the obstacle array exhibit opposite lateral drifts. The separation efficiency is excellent provided that the obstacle array is of sufficient length. The spin and longitudinal flow of the rotors and the friction between rotors and obstacles jointly determine the lateral drift of the rotors, thus leading to chiral separation. Furthermore, we propose a simple theoretical model, which captures the essential mechanism underlying the chiral separation and properly reproduces the experimental critical collision angle. This scheme could separate objects with static chiral structures, once an external source can power the objects to spin with different angular velocities.

* Corresponding author at: Beijing National Laboratory for Condensed Matter Physics and Laboratory of Soft Matter Physics, Institute of Physics, Chinese Academy of Sciences, Beijing 100190, China.
** Corresponding author.
E-mail addresses: mcyang@iphy.ac.cn (M. Yang), ningzheng@bit.edu.cn (N. Zheng).

https://doi.org/10.1016/j.powtec.2022.117671
Received 5 April 2022; Received in revised form 27 May 2022; Accepted 20 June 2022
Available online 23 June 2022

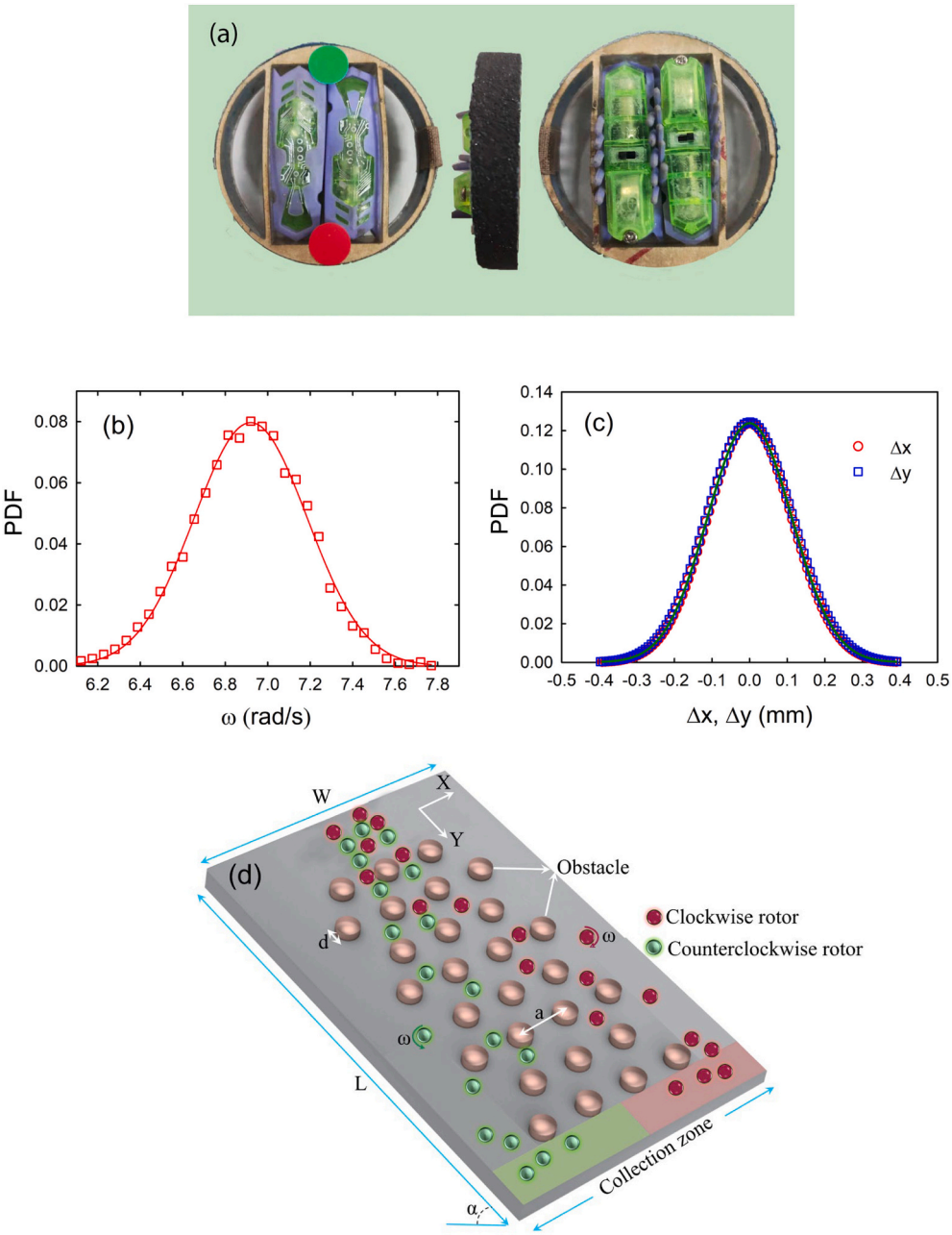

Fig. 1. (a) An active rotor consists of two Hexbug robots and an acrylic disk shell: top view, side view and bottom view, from left to right. (b) and (c) Probability distribution functions of the angular velocity and displacement components of a single rotor. The full lines are fits with Gaussian distribution. (d) Schematic diagram of the experimental system.

1. Introduction

In active matter, constituent particles convert their own or ambient energy into directed motion on an individual scale [1,2]. The directed motion not only includes the translational self-propulsion, but also the directional rotation. Depending on the characteristics of motion, active particles can be categorized into linear active particles (with directional translation and stochastic rotation), circular active particles (with both directional translation and unidirectional rotation) and active rotors (with stochastic translation and directional rotation). In particular, the directed rotation breaks both time-reversal and parity symmetries, such that the active rotors are often called chiral active particles. Chiral active matter can exhibit novel behaviors. For instance, a crowd of rotors possess a nondissipative transport coefficient called “odd viscosity” or “Hall viscosity” [3,4], and active rotors in the confinement can exhibit robust boundary flow, which is closely related to quantum Hall fluid and topological insulator.

Active particles are, in most cases, studied in a complex environment, generally including confined geometry, boundary walls, obstacles, etc. [5]. The particle's activity and environmental complexity can jointly result in the emergence of the spatiotemporal structures and exotic collective dynamics observed in active systems [6–17], which are not present in the equilibrium state. The study of these intriguing properties provides promising chances to uncover new physics and, simultaneously, to develop novel strategies for designing smart devices and advanced materials.

Obstacles, as a typical class of complex environment, can induce various counterintuitive motion behaviors such as directional transport, super-diffusion, sub-diffusion, and even trapping when interacting with active particles [18–25]. Based on these interesting behaviors, a series of

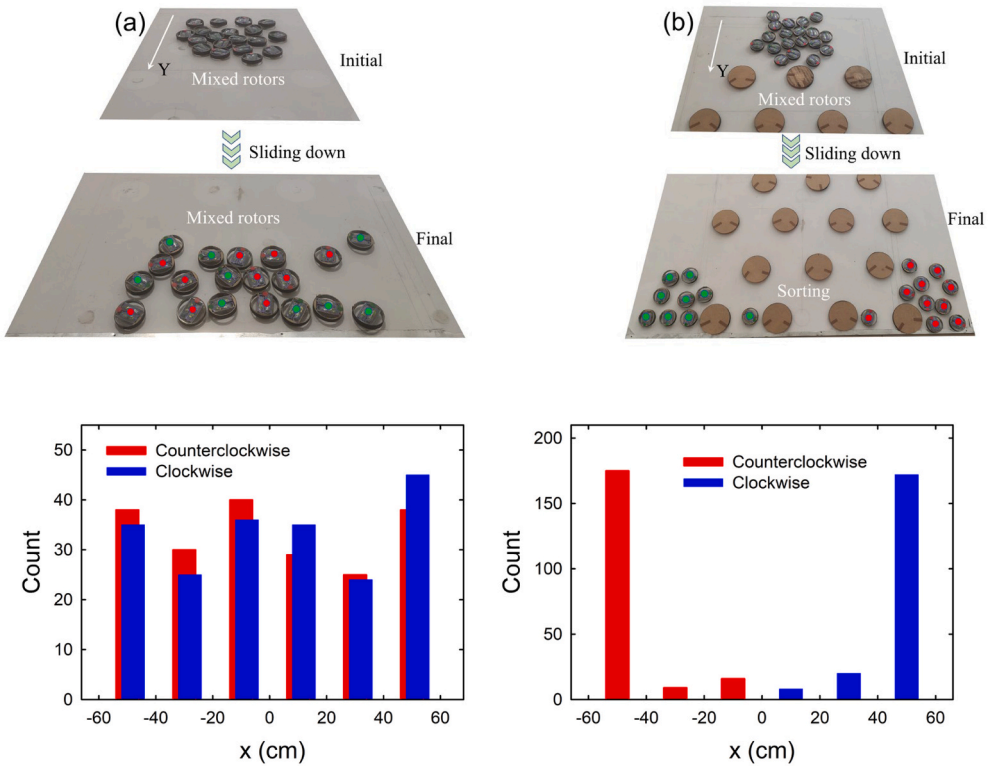

Fig. 2. Mixture of chiral rotors sliding down to the bottom of the inclined plate, and histograms of 200 rotors at various lateral position of the bottom of the inclined plate. (a) without obstacles, still showing the mixed state. The origin corresponds to the center of the plate. (b) with obstacles, showing chiral separation.

complex functions ranging from rectification, separation, and capture to sorting of particles are realized by designing the arrangement of obstacles, the structure of obstacles, and interactions between obstacles and particles [26–35]. Among these applications, the separation or sorting of active particles is of crucial importance for various fields in science and engineering.

Previous studies have reported the sorting or separation of linear active or circular active particles in an obstacle array [26,29–31,34–37], originating from the interplay between the motion attributes of active particles (i.e., the persistent length, chiral rotation and so on) and obstacles. However, research on the separation of active rotors is rare, although the rotor is also a common type of active particle. In contrast, recent study has focused more on collective movement and self-organization of active rotors in the absence of obstacles [38–42].

In this paper, we experimentally construct a system to separate active rotors with different chirality, i.e., spin direction. Specifically, patterned obstacles are fixed on an inclined plate, and mixed chiral rotors (clockwise and counterclockwise spin) slide down the plate and pass through the obstacle array. Our experiment unambiguously demonstrates that a rotor is always displaced laterally after the rotor bumps into an obstacle. The direction of the transverse transport depends on the chirality of rotation. Thus, clockwise and counterclockwise rotors are chirally separated to opposite sides of the inclined plate after they pass through the obstacle array. We also find that the separating effect strongly depends on the friction between rotors and obstacles. Furthermore, we propose a simple theoretical model that can properly reproduce the characteristics of the chiral separation achieved in experiments and thus reveal its essential mechanism.

2. Experimental setup

The active rotor in the experiment consists of two Hexbug robots and an acrylic disk shell. A single Hexbug robot, with a length of 4.5 cm and width of 1.3 cm, carries a 1.5 V button cell battery that drives a built-in vibration motor, which has been used in previous studies [14,43–47]. There are 5 pairs of parallel, flexible rubber legs on each side of the robot's body, and all legs bend slightly backward. The vibration motor, through the flexible legs, can drive the robot to perform approximately linear motion just perturbed by random noise on a two-dimensional solid substrate. The random noise, consisting of internal and environmental noise, can result from the noise of the vibration motor inside the robot, the nonuniform friction between the rotor and the substrate, a slight length difference between the ambilateral legs of the rotor, etc. Two Hexbug robots arranged in antiparallel directions, are installed in an acrylic disk shell of diameter 5.5 cm, forming an active rotor, as shown in Fig. 1 (a). The arrangement configuration of two robots will lead to a torque that spins the rotor. By exchanging the positions of two robots, we can change the chirality of a rotor, i.e., from clockwise to counterclockwise spin and vice versa. An individual rotor in a plane with no obstacles spins with an average angular velocity $\omega \approx 6.9 rad/s$, see Fig. 1 (b), where the probability distribution function of the angular velocity is symmetrical with respect to 6.9 rad/s. Similarly, the distribution of translational displacement of a single rotor is symmetrical with respect to the origin [see Fig. 1 (c)], suggesting that the rotor performs an unbiased Brownian motion.

The experimental system, consisting of an inclined plate (length $L = 180$ cm, width $W = 120$ cm, and an inclined angle α) and a two-dimensional cylinder (i.e., obstacles) array, can separate and collect active disk-shaped rotors with opposite spin chirality sliding through the obstacles, as shown in Fig. 1 (d). The rotors with opposite chirality are uniformly mixed and placed on the top of the slanted plate. Initially, these rotors are restricted by a baffle. Then the baffle is removed and the rotors slide down the plate and pass through the obstacle array attached to the plate. The arrangement pattern of the obstacles is a triangular lattice, and the center-to-center distance between two neighboring posts is $a = 22$ cm, with obstacle diameter $d = 10$ cm.

The coefficient of friction between the rotor and obstacle is tuned by pasting sandpapers with various roughness on the outer side faces of the

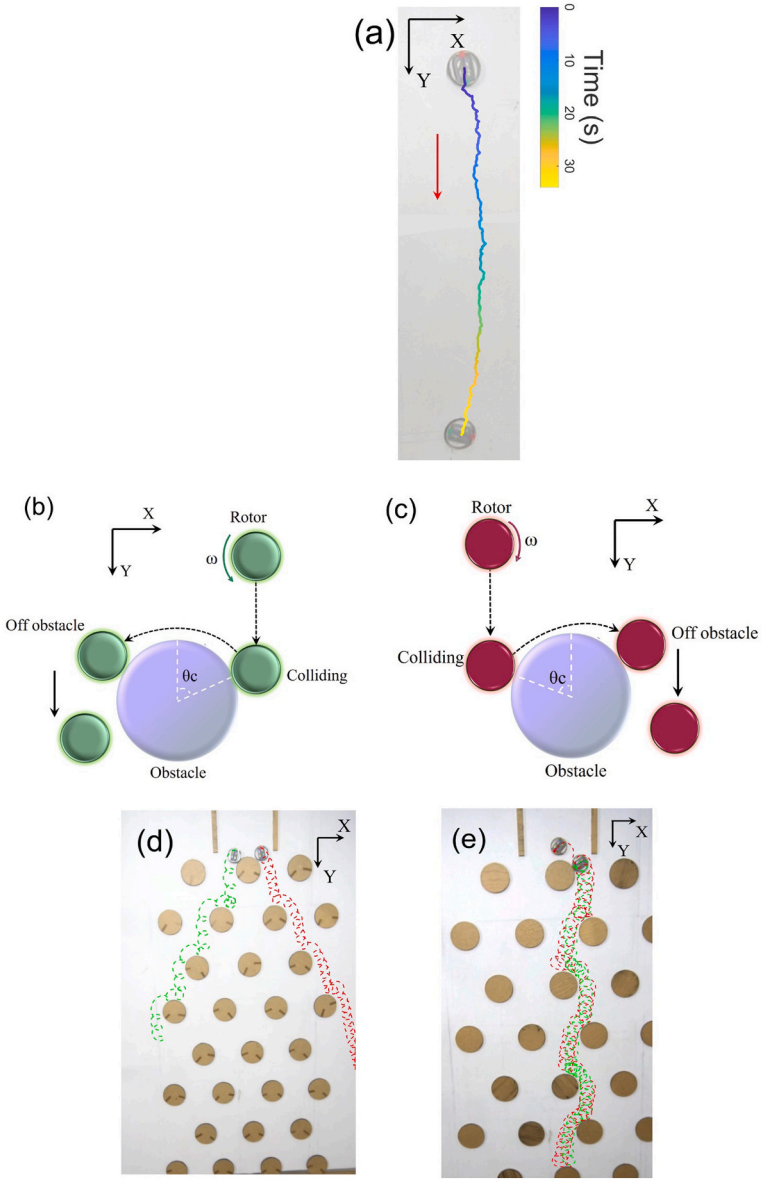

Fig. 3. (a) The approximate straight-line trajectory of a rotor sliding down the plate without obstacles. Color bar indicates time. (b) and (c) deflection in the lateral direction (+*x* or -*x* direction) as a counter-clockwise (clockwise) rotor colliding with an obstacle. Trajectories are spiral because the tracing point on the rotor is off the rotor's center. (d) dependence of the direction of the lateral drift on the spin chirality (rotor against rough surface). (f) almost no lateral drift (rotor against smooth surface).

rotor shell and obstacle. Here, two methods are applied to quantitatively determine the coefficient of friction. In the first method, a sandpaper is glued on the bottom of a sleigh, and the sleigh is put on an inclined surface covered by the same sandpaper. The inclined angle is measured to obtain the coefficient of friction as the sleigh starts to slide. To measure the friction coefficients by the second method, a sandpaper is pasted on the flat bottom of a metal block with a mass *M*, and a string is attached to the block. On the other end of this string, a weight with a mass of *m* is hung via a pulley to apply a force *mg*. The applied force pulls the block with a constant acceleration, and the coefficient of friction can be given by $\mu = \frac{mg-(M+m)a}{Mg}$, where *m*, *M* and *a* (i.e., the acceleration of the block or weight) can be directly measured experimentally. The two methods, thus, can be cross tested to acquire a reliable coefficient of friction between the rotor and the obstacle. A digital camera hung above the inclined plate records the trajectories of the sliding rotors, the contact position of a rotor colliding with an obstacle, and the number of rotors in the collection area at the bottom of this plate for the following data analysis. Each experiment runs about 30 min.

3. Experimental results

3.1. Chiral separation of rotors passing through the obstacle array

We release 20 rotors uniformly mixed, 10 clockwise and 10 counterclockwise, from the top of the inclined plate. These rotors slide down to the bottom of the inclined plate without the obstacles array, still remaining mixed. Namely, two kinds of chiral rotors distribute in each collection area, as shown the Fig. 2 (a).

In contrast, mixed rotors pass through the obstacles array, and spontaneously separate into two groups according to their spin chirality. The counterclockwise rotors accumulate on the collection area that is on the left side of the bottom of the inclined board, and the clockwise ones on the right collection area. The separating efficiency is 1, i.e., the two kinds of chiral rotors are completely separated and respectively collected, see Fig. 2 (b). For the separation of chiral rotors, we examined the effect of several arrangement patterns of obstacles, such as rectangular and parallelogram lattice, on the separating efficiency. It is found that as long as the row number of the obstacle array is sufficient and the gap between neighboring obstacles will not cause rotor clogging, the efficiency is independent of the arrangement pattern and is almost 1. For

the present the obstacle pattern, the minimum number of obstacle rows required to achieve a chiral separation is estimated by $m = \left[\frac{W}{2d}\right] + 1$, where W is the width of the inclined plate, d is the diameter of the obstacle, and […] represents a rounding symbol. Generally, the minimum number of obstacle rows is determined by the pattern configuration, the obstacle geometry, and the lateral shift of rotors. In addition, we investigate the effect of the rotor number on the separating efficiency. The random collision between rotors significantly increases with the rotor number, which is obviously unfavorable to the separation. However, we once again find the separation will be complete when the number of obstacle rows is sufficient; that is, an excellent separating efficiency can always be eventually obtained. The above experiments suggest that the emergence of the separation phenomenon is very robust when the rotors pass through the obstacle array.

3.2. Trajectory of a rotor after collision with an obstacle

If there are no obstacles on the inclined plate, a rotor will slide down the plate in a nearly-straight trace, approximately parallel to the y direction, as shown in Fig. 3 (a) where the center of the rotor is tracked. However, provided that obstacles are present on the plate, the motion behaviors of the rotors will be different. For example, when a counterclockwise rotor collides with an obstacle, even if the collisional position is located at the right side of the obstacle (i.e., biased towards the $+x$ direction with respect to the central line of the obstacle), the rotor will rotate against the obstacle and move to the opposite side of the obstacle until it is detached from it, as illustrated in Fig. 3 (b). As the rotor collides with next obstacle, the deflection in the lateral direction ($-x$ direction) often repeats, eventually resulting in a net lateral migration for the rotor. In contrast, a clockwise rotor always tends to move towards the $+x$ direction after a collision, see Fig. 3 (c). If there are multiple rows of obstacles on the plate, there will be an obvious lateral deflection in the $+x$ direction after multiple collisions of the rotor with obstacles. So, the direction of the lateral drift depends on the chirality of rotation, as shown in Fig. 3 (d).

3.3. Friction between a rotor and obstacle

It is experimentally observed that the inter-rotors collisions cause some rotors to deviate from their original trajectories. However, if the row number of obstacles is enough, those rotors will always return to the direction they should deflect, showing that the inter-rotor collisions do not qualitatively affect the separating results. This implies that the interactions between the rotors and obstacles, instead of the interactions between the rotors, causes the chiral separation.

Since the transverse migration of the rotor is a single-particle effect and arises from the collisions of the spinning rotor with the obstacle, it can be speculated that the friction coupling between the rotor and obstacle play a key role. To see this, we change the friction coupling between the rotor and obstacle. As rough sandpapers are pasted on side surfaces of a rotor and obstacle (the coefficient of friction between them is about 0.7), the trajectory of the rotor after a collision is consistent with that in Fig. 3 (b) and (c). If the rough sandpaper is replaced by a smooth Teflon tape (the coefficient of friction between them is about 0.1), most rotors, whether clockwise or counterclockwise rotation, slide along the collisional side of the obstacle and hardly move to the opposite side (except when the collisional position is near the central line of the obstacle). In this case, the lateral drift along the x direction is small or negligible, as shown in Fig. 3 (e).

4. Theoretical model

As stated above, after a rotor collides with an obstacle, the coupling of spin and friction between the obstacle and rotor, can cause the biased lateral motion of the rotor in the x direction. One of the crucial conditions for chiral separation is that the rotor can overcome the sliding gravity and "climb" back to the biased direction to which it should laterally move, even if the collisional position is at the opposite side of the obstacle.

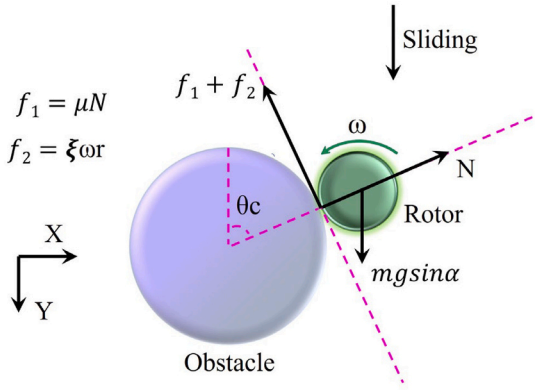

Fig. 4. A close-up sketch showing the force and torque balance of a single counterclockwise rotor at a critical angle θ_c.

The experimental observation shows that there exists a critical collisional position at the obstacle. If the collisional point is not beyond the critical position, the rotor, clinging to the obstacle after collision, can circle to the other side of the obstacle until it is detached from the obstacle. However, if a rotor collides the area off the critical position, it will not laterally migrate to the opposite side of the obstacle, but continue to slide along the obstacle until it leaves the obstacle. Here, we introduce a critical angle θ_c to describe the critical collisional position, where θ_c is defined as an acute angle between the direction of the normal force N exerted on the obstacle by the rotor, and the y direction on the plate, as shown in Fig. 4 (a). Apparently, θ_c is related to the motion parameters of the rotor itself, the inclined angle of the plate, and the frictional coefficient between the rotor and obstacle.

To clarify the underlying mechanism of the lateral drift of the rotor, a simple theoretical model is constructed based on the experimental observation that the rotor, against the obstacle after a collision, can circle to the other side of the obstacle. Assuming that the motion of the rotor against the obstacle is rolling without slipping, force and torque balance conditions of the rotor hold and are established as follows (Note that the following balance equations are only valid for the critical position).

$$mgsin\alpha sin\theta_c = \mu N + \xi \omega r \tag{1}$$

$$N = mgsin\alpha cos\theta_c \tag{2}$$

Torque balance shows,

$$M - \mu N r - \eta \omega = 0 \tag{3}$$

Where m is the mass of the rotor, ξ translational frictional coefficient between the rotor and inclined plate, η rotational frictional coefficient between the rotor and inclined plate, N normal force between the rotor and obstacle, α the inclined angle of the plate, θ_c the critical angle between the direction of the normal force N and the x direction on the plate, ω angular velocity of the rotor, M the rotational torque of the rotor, r the radius of the rotor, and μ the frictional coefficient between the rotor and obstacle. When writing down Eqs. (1) and (3), we have assumed that the maximum static friction between the rotor and obstacle is equal to the sliding friction μN.

The critical angle θ_c can be solved by combining Eqs. (1)–(3),

$$\theta_c = arccos\left[\frac{m'^2 - (Mkr)^2}{m'\left(MkrQ + \sqrt{m'^2 + m'^2Q^2 - M^2k^2r^2}\right)}\right] \tag{4}$$

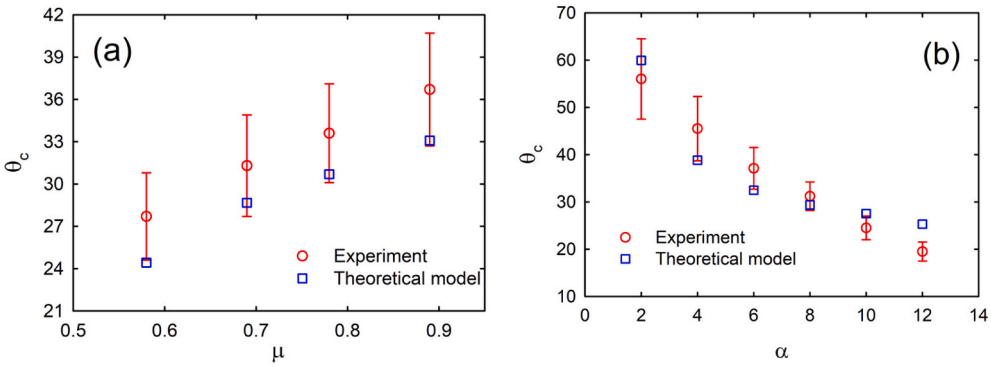

Fig. 5. Comparison of the critical angle obtained from experiment and theoretical calculation. The critical angle θ_c as a function of (a) μ with $\alpha = 7^0$and (b) the inclined angle α with $\mu = 0.78$.

Where $Q = \mu - \mu k r^2$, $m^{'} = mg \sin\alpha$ and $k = \frac{\xi}{\eta}$. The parameters in Eq. (4) are obtained from experimental measurements [14], with $m = 20.95g$, $r = 2.5$ cm. $M = 2.2 \times 10^{-4} N \cdot m$, $\xi = 0.21 kg/s$ and $\eta = 2.48 \times 10^{-4} kg \cdot m^2/s$. In experiments, four kinds of sandpapers with various roughness are used to change the friction between the rotor and obstacle, and the frictional coefficient μ is 0.58 ± 0.02, 0.69 ± 0.02, 0.78 ± 0.02 and 0.89 ± 0.03, respectively. In the experiment, the critical angle is determined as follows. Let one rotor slide down and collide with an obstacle fixed on the plate, and measure the maximum angle where the rotor can barely move from the collisional side to the opposite side of the obstacle.

Fig. 5(a) shows that the critical angle θ_c increases with frictional coefficient μ, when the inclined angle of the plate α is given. On the other hand, for a fixed μ, θ_c drops with the increase of α, as plotted in Fig. 5 (b). The theoretical results agree well with the experimental measurements. The theoretical model, without any fitting parameter, properly reproduces the critical angle, indicating that it correctly captures the physical essence of the chiral separation of the rotor mixture. Nevertheless, the theoretical model is deterministic and does not account for the stochasticity of the rotor motion, which can originate from the less-than-perfect spin of a rotor due to asymmetry of two robots in the rotor, imperfect collisions between rotors and obstacles, and random collisions from other rotors. In addition, inelastic collisions between the rotor and the obstacle seem important for the use of Eqs. (1)–(3), otherwise the rotor can bounce off and the balance equations will be invalid.

5. Conclusion

In summary, we experimentally realize chiral separation of a mixture of disk-shaped active rotors by externally driving them through an obstacle array. The separating efficiency will be complete when the row number of the obstacle array is sufficient. We find that the spinning direction of the rotor and its frictional interaction with the obstacles determine the direction of lateral drift of the rotors, thus leading to chiral separation. Furthermore, we put forward a simple theoretical model, which captures the essential mechanism underlying the chiral separation and properly reproduces the experimental data of the critical collision angle, without free parameters.

The system for separating chiral rotors is structurally simple and easy to operate. When the obstacle rows and friction between the rotor and obstacle are appropriate, high-quality separation can be achieved. Furthermore, this system also has the potential to be used to separate objects with static chiral structures, provided that an external vibration source or magnetic field can power the objects to rotate differently. In addition, chiral rotors with different surface roughness can also be separated according to this separation mechanism.

Author contributions

N. Zheng and W-J Li proposed methodology; W-J Li, L-F Li, Q-F Shi and N. Zheng performed data curation; N. Zheng and M-C Yang did formal analysis; N. Zheng and L-F Li proposed conceptualization, and N. Zheng and M-C Yang wrote the paper.

Declaration of Competing Interest

The authors declare that they have no known competing financial interests or personal relationships that could have appeared to influence the work reported in this paper.

Acknowledgements

We appreciate Jon P. Johnson for a critical reading of this paper. This work was supported by National Natural Science Foundation of China (Grant No.11974044 and 11874397).

References

[1] M.C. Marchetti, J.-F. Joanny, S. Ramaswamy, T.B. Liverpool, J. Prost, M. Rao, R. A. Simha, Rev. Mod. Phys. 85 (2013) 1143.
[2] C.J. Olson Reichhardt, C. Reichhardt, Annu. Rev. Condens. Matt. Phys. 8 (2017) 6.1–6.25.
[3] D. Banerjee, A. Souslov, A.G. Abanov, et al., Nat. Commun. 8 (1) (2017) 1–12.
[4] K. Dasbiswas, K.K. Mandadapu, S. Vaikuntanathan, Proc. Natl. Acad. Sci. U. S. A. 115 (39) (2018) 9031–9040.
[5] C. Bechinger, R. Di Leonardo, H. Löwen, C. Reichhardt, G. Volpe, G. Volpe, Rev. Mod. Phys. 88 (2016), 045006.
[6] D.A. Quint, A. Gopinathan. arXiv:1302.6564, 2013.
[7] A. Morin, N. Desreumaux, J.-B. Caussin, D. Bartolo, Nat. Phys. 13 (2017) 63–67.
[8] C. Reichhardt, C.J. Olson-Reichhardt, Soft Matter 10 (2014) 7502–7510.
[9] F. Kümmel, P. Shabestari, C. Lozano, G. Volpe, C. Bechinger, Soft Matter 11 (2015) 6187–6191.
[10] D.F. Hinz, A. Panchenko, T.-X. Kim, E. Fried, Soft Matter 10 (2014) 9082–9089.
[11] C. Reichhardt, C.J. Olson-Reichhardt, Phys. Rev. E 90 (2014), 012701.
[12] B.-Q. Ai, Y.-F. He, W.-R. Zhong, Soft Matter 11 (2015) 3852–3859.
[13] J. d'Dalessandro, A. Barbier-Chebbah, V. Cellerin, O. Benichou, R.M. Mège, R. Voituriez, B. Ladoux, Nat. Commun. 12 (2021) 4118.
[14] X. Yang, C. Ren, K. Cheng, H.P. Zhang, Phys. Rev. E 101 (2020), 022603.
[15] Q. Yang, H. Zhu, P. Liu, R. Liu, Q. Shi, K. Chen, N. Zheng, F. Ye, M. Yang, Phys. Rev. Lett. 126 (2021), 198001.
[16] M. Paoluzzi, R. Di Leonardo, L. Angelani, Phys. Rev. Lett. 115 (2015), 188303.
[17] S. Liu, S. Shankar, M.C. Marchetti, Y. Wu, Nature (London) 590 (2021) 80–84.
[18] A. Guidobaldi, Y. Jeyaram, I. Berdakin, V.V. Moshchalkov, C.A. Condat, V. I. Marconi, L. Giojalas, A.V. Silhanek, Phys. Rev. E 89 (2014), 032720.
[19] P.K. Ghosh, V.R. Misko, F. Marchesoni, F. Nori, Phys. Rev. Lett. 110 (2013), 268301.
[20] O. Chepizhko, F. Peruani, Phys. Rev. Lett. 111 (2013), 160604.
[21] T. Bertrand, Y. Zhao, O. Bénichou, J. Tailleur, R. Voituriez, Phys. Rev. Lett. 120 (2018), 198103.
[22] C. Reichhardt, C.J.O. Reichhardt, Phys. Rev. E 102 (2020), 042616.
[23] O. Chepizhko, E.G. Altmann, F. Peruani, Phys. Rev. Lett. 110 (2013), 238101.
[24] W.-J. Zhu, W.-R. Zhong, J.-W. Xiong, B.-Q. Ai, J. Chem. Phys. 149 (2018), 174906.
[25] K. Schakenraad, et al., Phys. Rev. E 101 (2020), 032602.

[26] G. Volpe, I. Buttinoni, D. Vogt, H.-J. Kümmerer, C. Bechinger, Soft Matter 7 (2011) 8810–8815.
[27] A. Kaiser, H.H. Wensink, H. Löwen, Phys. Rev. Lett. 108 (2012), 268307.
[28] A. Pototsky, A.M. Hahn, H. Stark, Phys. Rev. E 87 (2013), 042124.
[29] Q. Chen, B.-Q. Ai, J. Chem. Phys. 143 (2015), 104113.
[30] M. Mijalkov, Giovanni Volpe, Soft Matter 9 (2013) 6376.
[31] T. Barois, J.-F. Boudet, J.S. Lintuvuori, H. Kellay, Phys. Rev. Lett. 125 (2020), 238003.
[32] N. Kumar, R.K. Gupta, H. Soni, S. Ramaswamy, A.K. Sood, Phys. Rev. E 99 (2019), 032605.
[33] R. Martinez, F. Alarcon, J.L. Aragones, C. Valeriani, Soft Matter 16 (2020) 4739.
[34] J. Su, H. Jiang, Z. Hou, Soft Matter 15 (2019) 6830.
[35] L.-X. Wu, H.-W. Zhu, N. Zheng, Q.-F. Shi, Powder Technol. 391 (2021) 157–161.
[36] P. Forgács, A. Libál, C. Reichhardt, C.J.O. Reichhardt, Phys. Rev. E 104 (2021), 044613.
[37] M. Brun-Cosme-Bruny, A. Förtsch, W. Zimmermann, E. Bertin, P. Peyla, S. Rafaï, Phys. Rev. Fluids 5 (2020), 093302.
[38] N. Uchida, R. Golestanian, Phys. Rev. Lett. 104 (2010), 178103.
[39] N.H.P. Nguyen, D. Klotsa, M. Engel, S.C. Glotzer, Phys. Rev. Lett. 112 (2014), 075701.
[40] C. Scholz, M. Engel, T. Pöschel, Nat. Commun. 9 (2018) 931.
[41] P. Liu, et al., Proc. Natl. Acad. Sci. U. S. A. 117 (22) (2020) 11901–11907, 2.
[42] C. Scholz, A. Ldov, T. Pöschel, M. Engel, H. Löwen, Sci. Adv. 7 (2021) eabf8998.
[43] J.F. Boudet, J. Lintuvuori, C. Lacouture, T. Barois, A. Deblais, K. Xie, S. Cassagnere, B. Tregon, D.B. Brückner, J.C. Baret, H. Kellay, Sci. Robot. 6 (2021) eabd0272.
[44] G.A. Patterson, D. Sornette, D.R. Parisi, Phys. Rev. E 101 (2020), 042302.
[45] O. Dauchot, V. Démery, Phys. Rev. Lett. 122 (2019), 068002.
[46] R. Sánchez, P. Díaz-Leyva, Physica A (2018) 11–19.
[47] G.A. Patterson, P.I. Fierens, F.S. Jimka, P.G. König, A. Garcimartín, I. Zuriguel, L. A. Pugnaloni, D.R. Parisi, Phys. Rev. Lett. 119 (2017), 248301.